Automatic Pavement-Crack Detection and Segmentation Based on Steerable Matched Filtering and an Active Contour Model

Shuai Li[1]; Yang Cao[2]; and Hubo Cai, M.ASCE[3]

Downloaded from ascelibrary.org by SHENZHEN UNIVERSITY on 01/25/19. Copyright ASCE. For personal use only; all rights reserved.

Abstract: Cracks are an important symptom of pavement deterioration and deficiency. Accurate and complete information regarding pavement cracks is critical to determining pavement maintenance schedules, methods, and budgets. Two-dimensional (2D) pavement images are used in practice for crack detection and segmentation. Automatic crack detection and segmentation based on 2D images are challenging because of (1) low contrast between cracks and surrounding pavement; (2) complicated patterns of cracks; and (3) intensity inhomogeneity along cracks. To address these challenges, this paper presents a novel method to automatically detect and segment pavement cracks from 2D images. Specifically, the proposed method starts with the use of a steerable matched filter to generate a crack saliency map, which enhances the contrast between cracks and surrounding pavement and captures crack discontinuity and curvature. Analysis of the crack saliency map leads to a coarse crack region and rough estimates of crack properties. The coarse crack region is then fed into a region-based active contour model, and a level set evolution method is employed to implement the model for crack segmentation. The estimated crack properties provide information to automatically adjust the parameters of the active contour model for effective and efficient crack segmentation. The proposed method was tested using 65 pavement images with various cracks. The proposed method achieved average precision of 92.6%, recall of 85.1%, and F-measure of 88.7%. **DOI: 10.1061/(ASCE)CP.1943-5487.0000695.** © *2017 American Society of Civil Engineers.*

Author keywords: Pavement crack detection; Image processing; Steerable matched filter; Active contour model; Level set evolution.

Introduction

According to ASCE, 32% of America's main roads are in poor or mediocre condition (ASCE 2013). Effective and efficient pavement condition assessment is critical for transportation agencies to determine pavement maintenance schedules, methods, and budgets. Cracking is a common type of pavement distress, which is an important symptom of pavement deterioration and deficiency. Pavement cracks may be caused by vehicle overload, pavement self-aging, adverse weather conditions, and other factors, exhibiting different topological and geometric patterns and severity levels. The Federal Highway Administration (FHWA) conducted an assessment of pavement management practice that indicated that 94% of all state departments of transportation (DOTs) monitor cracking for the National Highway System (NHS) (FHWA 2015).

Conventionally, technicians need to identify the presence of pavement cracks from collected pavement data and segment the detected cracks for subsequent assessment. There are three main problems with manual crack detection and segmentation. First, it is nearly impossible for technicians to process all the collected data; thus only 10% are typically analyzed (Radopoulou and Brilakis 2016). Second, manual processing is time-consuming and labor-intensive. For instance, 60 full-time engineers are required to annually survey the 28,968-km (18,000-mi) Centerline Highway in the state of Georgia (Koch et al. 2012). Third, although manual processing is conducted based on well-defined guidelines and criteria, crack detection and segmentation still suffer from a high degree of subjectivity and poor reproducibility (Guan et al. 2015). Hence, many transportation agencies strive to automate the process of crack detection and segmentation.

Specialized vehicles are equipped with positioning systems, cameras, laser scanners, pavement profilers, and accelerometers to collect pavement data (Radopoulou and Brilakis 2016). The National Cooperative Highway Research Program (NCHRP) surveyed pavement distress collection practices from 43 state highway agencies, two FHWA offices, 10 Canadian provinces, and Transport Canada. It was reported that pavement surface images were collected through automated means by 30 agencies, whereas only 14 agencies employed automated methods to process the collected images (McGhee 2004). Tsai and Li (2012) further pointed out that only 8 North American highway agencies used automated crack detection in practice. With the proliferation of technologies, more transportation agencies are using automated techniques for pavement data collection. However, current data processing is still predominantly manual. In a recent study, Radopoulou and Brilakis (2016) estimated that only 0.4% of inspections are automatic and the remaining 99.6% are manual.

Two-dimensional (2D) pavement images are the main data source used in practice for crack detection and segmentation. Automatic crack detection and segmentation based on 2D images are challenging because of (1) low contrast between cracks and surrounding pavement (Zou et al. 2012); (2) complicated crack patterns (Li et al. 2011; Tsai et al. 2012); and (3) intensity inhomogeneity along cracks (Zou et al. 2012). This paper presents a novel method to automatically detect and segment pavement cracks from

[1]Ph.D. Candidate, Lyles School of Civil Engineering, Purdue Univ., 550 Stadium Mall Dr., West Lafayette, IN 47907. E-mail: li1155@purdue.edu

[2]Ph.D. Student, School of Building Construction, Georgia Institute of Technology, Atlanta, GA 30332. E-mail: ycao86@gatech.edu

[3]Associate Professor, Lyles School of Civil Engineering, Purdue Univ., 550 Stadium Mall Dr., West Lafayette, IN 47907 (corresponding author). E-mail: hubocai@purdue.edu

Note. This manuscript was submitted on November 30, 2016; approved on February 28, 2017; published online on May 29, 2017. Discussion period open until October 29, 2017; separate discussions must be submitted for individual papers. This paper is part of the ***Journal of Computing in Civil Engineering***, © ASCE, ISSN 0887-3801.

2D images which is robust to unfavorable conditions. The remainder of this paper is organized as follows. The next section reviews current research on automatic pavement crack detection and segmentation. Then the proposed crack detection and segmentation method is explained followed by a description of field experiments and results. Finally, research findings and contributions are highlighted and limitations and future research directions are pointed out.

Literature Review

Intensity-thresholding methods have been widely used for crack detection (Li and Liu 2008; Oliveira and Lobato Correia 2009; Kamaliardakani et al. 2014; Sun et al. 2015). However, background illumination and pavement texture significantly affect the performance of these methods, resulting in unreliable crack segmentation. Tsai et al. (2009) and Jiang and Tsai (2015) applied the algorithm created by Alekseychuk (2006) to segment pavement cracks. Alekseychuk's algorithm was developed to detect longitudinal crack-like indications in radiographic images; thus its performance may not be promising in segmenting cracks with complicated topology and geometry. Guan et al. (2015) showed that Alekseychuk's algorithm failed to segment a number of interconnected crack branches.

Zou et al. (2006) exploited a wavelet transform method to detect pavement defects. Ying and Salari (2010) proposed a beamlet transform–based technique to detect pavement cracks in which pavement images are partitioned into small windows and cracks are approximated using line segments. However, because of the anisotropic properties of wavelets, the wavelet-based method and its variants (Nejad and Zakeri 2011; Ouma and Hahn 2016) are not effective in extracting cracks with high curvature and poor continuity.

Region-growing methods are also common in crack segmentation. In the method by Huang and Xu (2006), crack seeds and clusters are verified by examining intensity and geometric characteristics such as shape, width, and length of potential crack regions. Li et al. (2011) proposed the F^* seed-growing approach that narrows the global searching space to improve efficiency. Gavilán et al. (2011) connected crack seeds by computing the paths with the lowest costs and the fewest symmetric restrictions. Li et al. (2014) used the Chan-Vese algorithm to segment cracks. These methods are subject to two limitations. First, region-growing methods require the placement of initial crack seeds, the selection of which significantly affects segmentation performance. Second, these region-growing methods are not robust to noise, intensity inhomogeneity, and complex topology with multiple branches.

Zou et al. (2012) and Guan et al. (2015) used tensor-voting methods to extract pavement cracks. Tensor voting first encodes input data as ball or stick tensors and then performs a voting process based on proximity information and continuation constraints from tensor to tensor. The crack pixels are identified by selecting the stick tensors with high votes. Although tensor voting can reveal saliency for crack points, directly extracting cracks from the saliency field requires users to tune the threshold parameters. Empirically tuned threshold values in Guan et al. (2015) and Zou et al. (2012) are not adequate to ensure consistent quality results for different pavement cracks in various environments.

Nishikawa et al. (2012) used iterative image filtering and genetic programming to detect cracks. However, both iterative filtering and genetic programming are computationally expensive. Yeum and Dyke (2015) used the Frangi filter and canny edge detector to extract cracks and removed spurious crack edges by examining eccentricity. Nguyen et al. (2014) pointed out that the Frangi filter is sensitive to noises that are prevalent in pavement images. Hence, in the region with a low signal-to-noise ratio, the Frangi filter may fail to detect small cracks and incorrectly classify noises as cracks. In addition, it cannot precisely localize the boundaries of cracks. Nguyen et al. (2014) employed phase symmetry to enhance the Frangi filter to remove noncrack objects. However, the use of phase symmetry is not adequate to completely address the problem because many noncrack objects also satisfy the phase symmetry constraint. Lins and Givigi (2016) proposed to detect cracks using a particle filter based on a color model context. Zalama et al. (2014) used the Gabor filter to detect longitudinal and transverse cracks. However, the design and the efficacy of their method remain ambiguous in detecting complex cracks such as alligator cracks.

Efforts have also been made in the field of artificial intelligence to detect pavement cracks. Cord and Chambon (2012) represented the textural information of pavement defects by a set of linear and nonlinear filters and performed supervised learning based on the AdaBoost algorithm to select the most pertinent filters for crack detection. The method proposed by Oliveira and Correia (2013) classifies nonoverlapping image blocks as either containing or not containing crack pixels based on a learning-from-samples paradigm. Prasanna et al. (2016) presented the spatially tuned robust multifeature classifier algorithm that uses curve fitting to spatially localize potential crack regions. All of these methods share two main limitations. First, they can only distinguish pavement images or subregions of a pavement image with defects from those without defects. Hence accurate segmentation of cracks is not attainable, preventing detailed assessment of pavement cracks. Second, the performance of these methods depends largely on the quantity and quality of training data. The acquisition of a large amount of high quality data is a main challenge for these methods.

Despite the advancements made by existing studies, automatic and accurate crack detection and segmentation are still challenging because of low contrast between cracks and surrounding pavement, complex crack patterns, and intensity inhomogeneity along cracks. These challenges have not been fully addressed because (1) existing methods are not adequate to capture cracks with high curvature given that most studies assume that cracks are straight lines; (2) existing methods cannot adapt themselves to detecting cracks with common, complicated patterns such as bifurcations; and (3) existing methods do not explicitly deal with intensity inhomogeneity along a crack, resulting in some misclassification of crack pixels as noncrack pixels. This study attempted to create a novel crack detection and segmentation method that is robust to the these unfavorable conditions.

Methodology

Fig. 1 is an overview of the proposed method that consists of three steps for crack detection and segmentation. Filters are useful in pavement crack detection. The same filter often needs to be rotated to different orientations, and the filter response needs to be calculated at each orientation. A steerable filter synthesizes filters of arbitrary orientations from linear combinations of basis filters, allowing one to steer a filter to any orientation and to determine the filter response as a function of orientation. In the first step, a steerable filter with two rotatable tails is used to process pavement images. The maximum filter response is selected, forming a crack saliency map where each pixel is associated with a numerical value indicating its conspicuity of being a crack pixel. The second step involves analysis of the crack saliency map, which outputs a coarse crack region and rough estimates of crack properties. In the third

Downloaded from ascelibrary.org by SHENZHEN UNIVERSITY on 01/25/19. Copyright ASCE. For personal use only; all rights reserved.

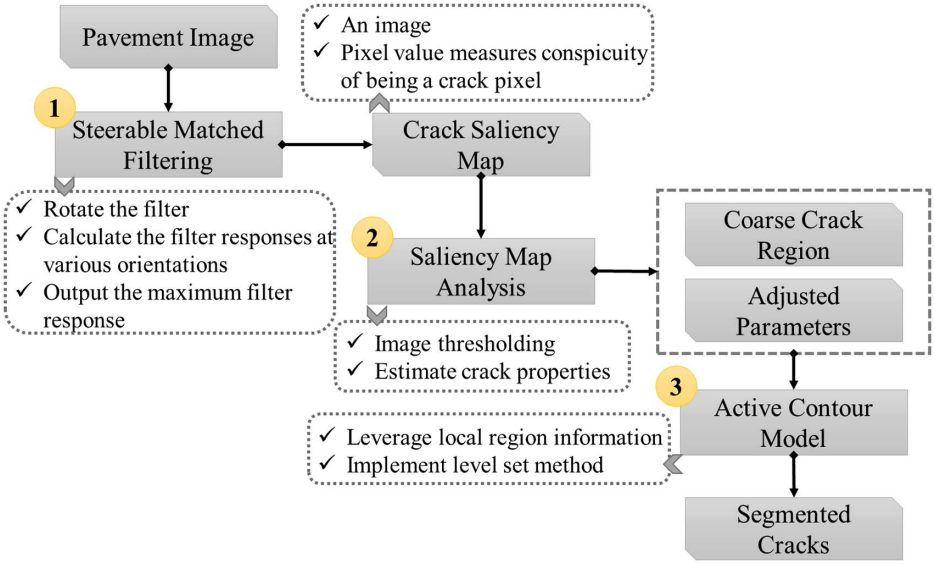

Fig. 1. Overview of the proposed method

step, the coarse crack region is fed into a region-based active contour model as a starting point for crack segmentation. The estimated crack properties provide information to automatically adjust the parameters of the active contour model. Via the level set method, the initial crack region continues to evolve by incorporating crack pixels even in the presence of complex crack patterns and intensity inhomogeneity. Next, the technical details of the proposed method are elaborated.

Steerable Matched Filtering

The steerable filter proposed by Freeman and Adelson (1991) is a linear combination of Gaussian second derivatives which is adopted in this study as a basic filter. Eq. (1) gives the 2D Gaussian with variance σ_1 at position $p_0 = (x, y)$, and Eq. (2) gives its second derivatives. Eq. (3) shows the formulation of the filter $f(p; \sigma_1, \theta)$, where $\theta \in [-\pi/2, \pi/2]$ is the orientation of the filter:

$$g(p_0; \sigma_1) = \frac{1}{\sqrt{2\pi}\sigma_1} e^{-(x^2+y^2)/2\sigma_1^2} \tag{1}$$

$$\begin{aligned} g_{xx}(p_0) &= \frac{(x^2 - \sigma_1^2)e^{-(x^2+y^2)/2\sigma_1^2}}{\sqrt{2\pi}\sigma_1^5} \\ g_{yy}(p_0) &= \frac{(y^2 - \sigma_1^2)e^{-(x^2+y^2)/2\sigma_1^2}}{\sqrt{2\pi}\sigma_1^5} \\ g_{xy}(p_0) &= g_{yx}(p_0) = \frac{xye^{-(x^2+y^2)/2\sigma_1^2}}{\sqrt{2\pi}\sigma_1^5} \end{aligned} \tag{2}$$

$$f(p_0; \sigma_1, \theta) = g_{xx}\cos^2\theta + 2g_{xy}\cos\theta\sin\theta + g_{yy}\sin^2\theta \tag{3}$$

The ultimate filter consists of three parts. The middle part is the basic filter represented by Eq. (3), to which, based on the recommendation from Mukherjee and Acton (2015), two rotatable tails are attached. These two additional tails are the shifted version of the basic filter with relative rotating angle α. The shifted positions p_1 and p_2 are shown in Eq. (4), where d is the offset. The two tails are used to account for high curvature, local intensity variation, and bifurcation in complex cracks. Eq. (5) illustrates the formulation of the ultimate steerable filter. Fig. 2 shows three instances of the steerable filter:

$$\begin{aligned} p_1 &= [x - d\sin(\theta + \alpha), y + d\cos(\theta + \alpha)] \\ p_2 &= [x + d\sin(\theta + \alpha), y - d\cos(\theta + \alpha)] \end{aligned} \tag{4}$$

$$\begin{aligned} F(p; \sigma_1, \theta, \alpha) = f(p_0; \sigma_1, \theta) + f(p_1; \sigma_1, \theta + \alpha) \\ + f(p_2; \sigma_1, \theta + \alpha) \end{aligned} \tag{5}$$

Four rationales justify the use of the steerable filter in crack detection. First, a crack usually has two parallel edges with gradient directions 180° apart. This characteristic is referred to as antiparallel. The antiparallel edges are formed by piecewise curvilinear segments that can be represented by the filters shown in Fig. 2. Second, a crack has lower reflectance than pavement surface and thus is darker relative to the background. Fig. 3 shows the intensity profiles at the cross sections of four cracks. The intensity profile across a crack can be approximated by Gaussian shape. In this sense, the steerable Gaussian filter reasonably resembles a crack in terms of intensity at the cross section. Third, as shown in Fig. 2, the incorporation of the two rotatable tails accounts for high curvature and bifurcation in complex cracks. From the three points just presented, one can observe that the steerable filter possesses some intrinsic features of a curvilinear crack segment, making it an exceptional option for crack detection. Fourth, since the steerable filter is a linear combination of Gaussian second derivatives, its implementation is straightforward and computationally efficient (Jacob and Unser 2004).

Eq. (6) calculates the filter response at position p when convolving an image $I(p)$ with the filter. If the filter with a scale σ_1 and an orientation (θ, α) can match a crack segment in a pavement image, the inner product in Eq. (6) is high. Hence a high magnitude of the response indicates a high probability of the presence of a crack segment:

$$R(p; \sigma_1, \theta, \alpha) = F(p; \sigma_1, \theta, \alpha) \times I(p) \tag{6}$$

The matched filtering is to find σ_1, θ, and α to maximize the response R. In this study, the filtering is conducted with a fixed

Downloaded from ascelibrary.org by SHENZHEN UNIVERSITY on 01/25/19. Copyright ASCE. For personal use only; all rights reserved.

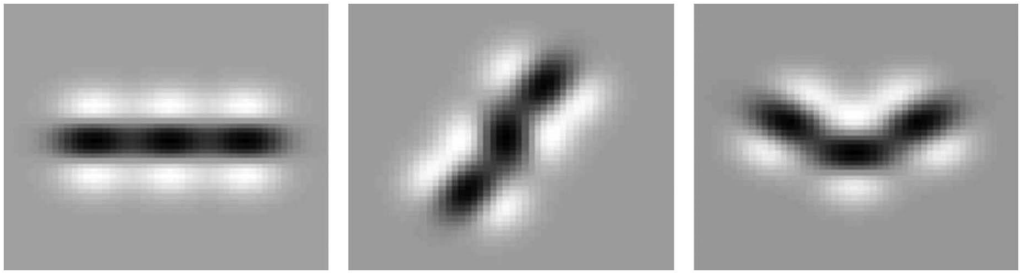

Fig. 2. Examples of the steerable filter

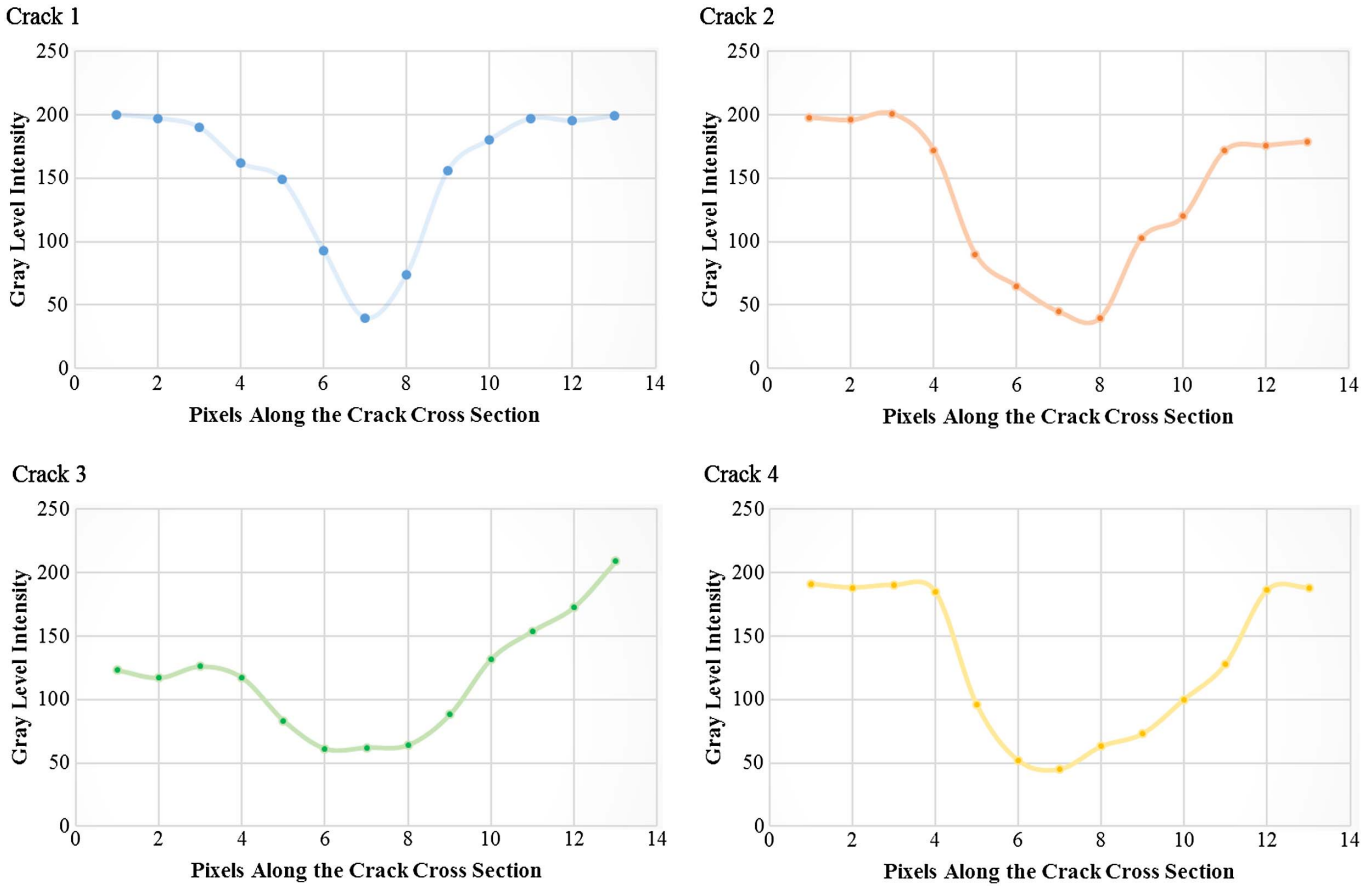

Fig. 3. Gray-level intensity profiles of the cross sections of four cracks

σ_1 to save computational effort. Eq. (7) illustrates the mathematical formulation of the optimization problem. It is solved numerically by searching the values of θ from $-\pi/2$ to $\pi/2$ and α from $-\pi/6$ to $\pi/6$ with a constant increment of $\pi/12$. The responses are calculated and compared, leaving only the maximum value:

$$R^*(p;\sigma) = \max_{\theta,\alpha} R(p;\sigma,\theta,\alpha) \tag{7}$$

The steerable matched filtering generates a crack saliency map. Fig. 4 shows two examples of the generated crack saliency map. In part because of pavement texture, some noncrack pixels also present high responses, which are not straightforward to suppress. In addition, some crack pixels have low responses because of the low contrast and intensity inhomogeneity. Extracting cracks directly from the crack saliency map is inaccurate. Therefore, a more sophisticated method is needed for crack segmentation.

Crack Saliency Map Analysis

Analysis of the crack saliency map leads to two important outputs: a coarse crack region and rough estimates of crack properties. The coarse crack region is an essential input for the region-based active contour model in the third step. The rough estimates of crack properties provide information to adjust the parameters of the active contour model to effectively and efficiently segment cracks.

To generate a coarse crack region, Otsu's thresholding method (Otsu 1975) is first applied to obtain a global threshold value. Then the standard deviation of filter responses is computed. To be conservative, the final threshold value is the sum of Otsu's threshold value and half of the standard deviation. Fig. 5 shows the coarse crack regions generated using the final threshold value. Based on the generated coarse crack region, rough estimates of the crack properties, including the number of crack segments and intersections, along with the total length of cracks are obtained. Specifically, the generated crack regions are first skeletonized and then

Downloaded from ascelibrary.org by SHENZHEN UNIVERSITY on 01/25/19. Copyright ASCE. For personal use only; all rights reserved.

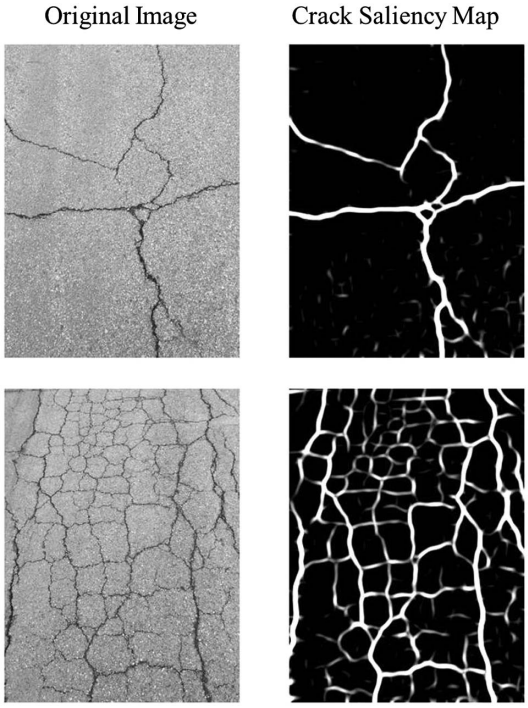

Fig. 4. Examples of generated crack saliency map

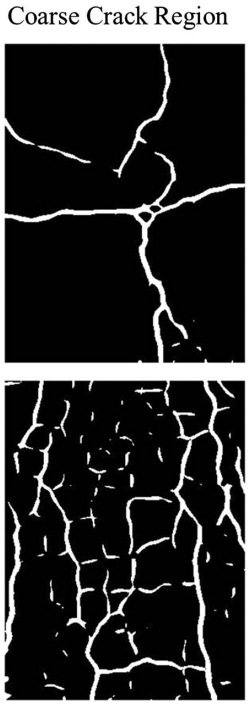

Fig. 5. Generated coarse crack regions

the intersections of the crack branches are identified, based on which cracks can be separated. The number of crack segments and the number of crack intersections are thus derived. The total length of cracks is estimated by counting the total pixels of crack edges.

Based on the estimated crack properties, cracks can be categorized into two groups: simple and complex. A simple crack, such as a longitudinal or a transverse crack, has a small number of crack branches and intersections and a short total crack length. A complex crack, such as a block or an alligator crack, has a large number of crack branches and intersections and a long total crack length. Segmenting simple and complex cracks deserves different parameter values in the active contour model. In this regard, the estimated crack properties can guide the algorithm to differentiate simple and complex cracks and subsequently self-adjust the parameters to effectively and efficiently extract cracks.

Active Contour Model

The active contour model based on region-scalable fitting energy proposed by Li et al. (2008) is employed in this study to segment pavement cracks because it uses local region information to address the intensity inhomogeneity challenge. This method is not robust with respect to initial contour selection. Moreover, segmentation performance is sensitive to the choice of parameters. The coarse crack region and rough estimates of crack properties derived from the crack saliency map provide valuable information to address the two limitations.

Fitting Energy

Let $I{:}\Omega \in \Re^2$ be the grayscale image of pavement, where $\Omega \in \Re^2$ denotes the image domain; C denotes a closed contour in the image domain Ω, which separates Ω into two regions: $\Omega_1 = \text{inside}(C)$ and $\Omega_2 = \text{outside}(C)$. For a given point $x \in \Omega$, the local intensity fitting energy is defined in Eq. (8). The values λ_1 and λ_2 are positive constants, and $f_1(x)$ and $f_2(x)$ approximate image intensities in Ω_1 and Ω_2, respectively. The value $K(x-y)$ is a Gaussian kernel defined in Eq. (9) which controls the size of a local region centered at the point x. The value $I(y)$ represents the intensities within the local region. The local intensity fitting energy E_x^{Fit} is a weighted mean square error of the approximation of the image intensities $I(y)$ outside and inside the contour C by the fitting values $f_1(x)$ and $f_2(x)$, respectively. The value $K(x-y)$ assigns a weight to each intensity $I(y)$ at y. Because of the localization property of the kernel function, the weight decreases and approaches zero as the point y goes away from the center point. Hence the fitting energy E_x^{Fit} is localized around the point x. The size of the local region is controlled by the parameter σ_2. A small σ_2 indicates that the fitting energy involves only the intensities within a small neighborhood of the point x, whereas a large σ_2 implies that the fitting energy involves the intensities in a large region centered at x:

$$E_x^{\text{Fit}}[C, f_1(x), f_2(x)] = \sum_{i=1}^{2} \lambda_i \int_{\Omega_1} K(x-y)|I(y) - f_i(x)|^2 dy \quad (8)$$

$$K_{\sigma_2}(Z) = \frac{1}{(2\pi)^{n/2}\sigma_2^n} e^{-|z|^2/2\sigma_2^2} \quad (9)$$

When the contour C is exactly on the crack boundary and the fitting values f_1 and f_2 optimally approximate the local image intensities on the two sides of C, the fitting energy E_x^{Fit} can be minimized. To obtain the entire crack boundary, a contour C needs to be identified to minimize the energy E_x^{Fit} for all x in domain Ω. In addition, most active contour models require smoothing of the contour C by penalizing its length $|C|$. Hence the crack boundary can be identified by minimizing the energy functional for a contour C in Eq. (10)

$$E[C, f_1(x), f_2(x)] = \int E_x^{\text{Fit}}[C, f_1(x), f_2(x)]dx + \nu|C| \quad (10)$$

Level Set Method

To solve the optimization problem, the level set method (Osher and Sethian 1988) is used. The evolving contour C is represented by the

Downloaded from ascelibrary.org by SHENZHEN UNIVERSITY on 01/25/19. Copyright ASCE. For personal use only; all rights reserved.

zero-level set of a Lipschitz function ϕ:$\Omega \rightarrow \Re$. The level set function ϕ takes positive and negative values outside and inside the contour C, respectively. Let H_ε be the smooth Heaviside function and δ_ε be the derivative of H_ε, defined in Eqs. (11) and (12):

$$H_\varepsilon(x) = \frac{1}{2}\left[1 + \frac{2}{\pi}\arctan\left(\frac{x}{\varepsilon}\right)\right] \tag{11}$$

$$\delta_\varepsilon(x) = H'_\varepsilon(x) = \frac{1}{\pi}\frac{\varepsilon}{\varepsilon^2 + x^2} \tag{12}$$

The energy functional in Eq. (10) can then be reformulated and approximated in Eq. (13), where $M_1^\varepsilon(\phi) = H_\varepsilon(\phi)$ and $M_2^\varepsilon(\phi) = 1 - H_\varepsilon(\phi)$:

$$E_\varepsilon(\phi, f_1, f_2) = \sum_{i=1}^{2} \lambda_i \int \left\{ \int K_\sigma(x-y)|I(y) - f_i(x)|^2 M_i^\varepsilon[\phi(y)]dy \right\} dx + \nu \int |\nabla H_\varepsilon[\phi(x)]|dx \tag{13}$$

A level set regularization term is introduced in Eq. (14) to preserve the regularity of the level set function ϕ. The level set regularization term characterizes the deviation in the function ϕ from a signed distance function. The introduction of a level set regularization term is necessary for accurate computation and stable level set evolution.

$$P(\phi) = \int \frac{1}{2}(|\nabla\phi(x)| - 1)^2 dx \tag{14}$$

Then the problem is to minimize the energy functional in Eq. (15), where μ is a positive constant:

$$F(\phi, f_1, f_2) = E_\varepsilon(\phi, f_1, f_2) + \mu P(\phi) \tag{15}$$

The gradient descent method is used to minimize the energy functional. For a fixed level set function ϕ, Eq. (16) gives $f_1(x)$ and $f_2(x)$ that minimize the energy functional in Eq. (15):

$$f_i(x) = \frac{\int K_\sigma(x-y) I(y) M_i^\varepsilon[\varphi(y)]dy}{\int K_\sigma(x-y) M_i^\varepsilon[\varphi(y)]dy} \, i = 1,2 \tag{16}$$

By fixing $f_1(x)$ and $f_2(x)$, the minimization of energy functional $F(\varphi, f_1, f_2)$ can be achieved by solving Eq. (17), the gradient descent flow equation, where $e_i(x) = \int K_\sigma(y-x)|I(x) - f_i(y)|^2 dy$:

$$\frac{\partial\phi}{\partial t} = -\delta_\varepsilon(\phi)(\lambda_1 e_1 - \lambda_2 e_2) + v\delta_\varepsilon(\phi)\mathrm{div}\left(\frac{\nabla\varphi}{|\nabla\varphi|}\right) + \mu\left[\nabla^2\phi - \mathrm{div}\left(\frac{\nabla\varphi}{|\nabla\varphi|}\right)\right] \tag{17}$$

Implementation

The level set function is initialized as a binary step function, which takes a negative constant value $-c_0$ inside the coarse crack region and a positive constant value c_0 outside the coarse crack region for a constant $c_0 > 0$. The merit of using the generated coarse crack region to initialize the level set function is twofold. First, the coarse crack region provides a good starting point that overcomes the limitation of many active contour models in selecting the initial contour. Second, using a binary step function can expedite curve evolution.

The number of iterations is a critical parameter in the level set evolution. Increasing the number of iterations can improve the precision of crack segmentation. For simple cracks, a small number of iterations are adequate to achieve a satisfactory segmentation. For complex cracks, a large number of iterations are required to attain a reasonable performance. The term $\nu\delta_\varepsilon(\phi)\mathrm{div}(\nabla\phi/|\nabla\phi|)$ has a length-shortening or a smoothing effect on the zero-level contour. A higher value produces a smoother contour. For simple cracks such as longitudinal and transverse cracks, the length of each crack segment is relatively long and its curvature is small. Hence a high value of ν should be used to segment simple cracks. For complex cracks such as block and alligator cracks, the length of each crack segment is short and its curvature can be large. Therefore, a low value of ν should be used to encompass small crack branches with high curvature. In addition, a smaller-scale σ_2 can enable the algorithm to localize crack boundaries more precisely, which is more suitable for segmenting complex cracks. Once the final segmentation is obtained, the cracks are pruned by removing small round objects. Fig. 6 shows the final extracted cracks using the level set method.

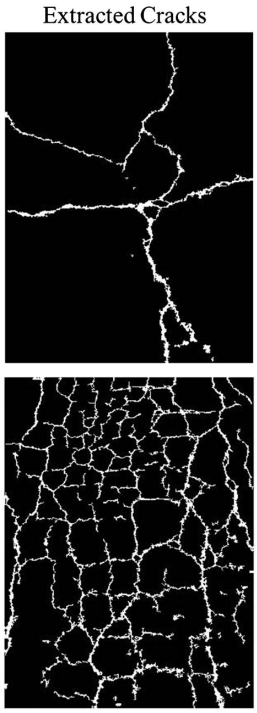

Fig. 6. Extracted cracks

Experiments and Results

With the use of an IPhone 6S, 65 pavement images were collected at Purdue University which contained longitudinal, transverse, block, and alligator cracks. The IPhone's camera was positioned at an approximate height of 1 m above the pavement surface and at an approximate orientation of 45°. The shadows cast by roadside objects were avoided when obtaining the images. The images were taken in fair weather, (i.e., during daylight in sunny or cloudy conditions). The frame size provided by this camera is 4,040 × 3,030 pixels. To save computational effort and also preserve adequate details for crack detection and segmentation, the images were resized to 404 × 303 pixels. The PC for processing the images had the following characteristics: Intel Core i7-3940XM, 3.00 GHz CPU, and 32 GB RAM.

The proposed method requires specification of a number of parameters that need to be numerically calibrated; here 25 pavement images were used for calibration. For the steerable matched

Downloaded from ascelibrary.org by SHENZHEN UNIVERSITY on 01/25/19. Copyright ASCE. For personal use only; all rights reserved.

filtering, the filter size was set to $3\sigma_1 \times 3\sigma_1$. Therefore, the entire Gaussian bell was taken into account. In addition, the filter decayed to nearly zero at the edges of the mask which avoided discontinuity in the filtered image. The offset parameter d was fixed as $0.5\sigma_1$. Hence the parameter to be tuned in the steerable matched filtering was the Gaussian variance σ_1. For the active contour model, the kernel was truncated as a $w \times w$ mask to compute the convolutions, where w was the smallest odd number no less than $4\sigma_2$. In addition, both λ_1 and λ_2 were 1. The parameters to be tuned in the active contour model were σ_2, ν, and the number of iterations. In the calibration, these parameters were tuned until the segmented cracks were visually close to the manually labeled cracks. Empirically, $\sigma_1 = 4$ was adopted in the experiments. For complex cracks, the value of σ_2 was 2 and $\nu = 0.003 \times 404 \times 303$, whereas for simple cracks the value of σ_2 was 6 and $\nu = 0.009 \times 404 \times 303$. The number of iterations for complex crack was 100, and that for simple cracks was 40. Fig. 7 shows 8 examples of the extracted cracks.

In this study, precision, recall, and F-measure were used to evaluate the performance of the proposed method. Precision measures the exactness or fidelity of detection and segmentation and is

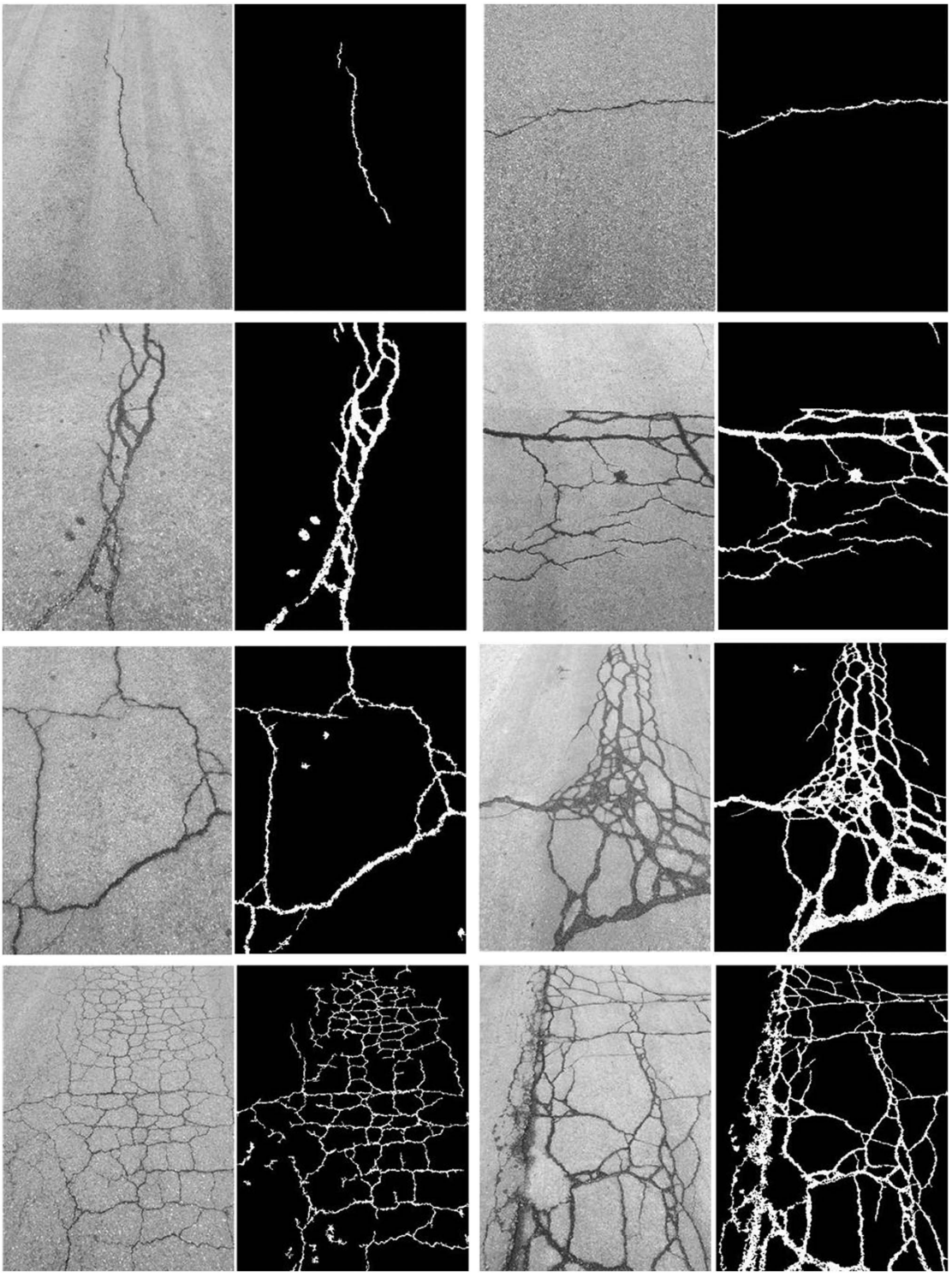

Fig. 7. Examples of crack detection and segmentation

Downloaded from ascelibrary.org by SHENZHEN UNIVERSITY on 01/25/19. Copyright ASCE. For personal use only; all rights reserved.

calculated in Eq. (18). Recall describes the completeness of detection and segmentation and is defined in Eq. (19). F-measure combines precision and recall and is computed in Eq. (20)

$$\text{Precision} = \frac{TP}{TP + FP} \tag{18}$$

$$\text{Recall} = \frac{TP}{TP + FN} \tag{19}$$

$$F\text{-measure} = 2 \times \frac{\text{precision} \times \text{recall}}{\text{precision} + \text{recall}} \tag{20}$$

In Eqs. (18) and (19), TP denotes true positives—that is, pixels labeled as crack pixels in the ground truth are correctly detected as crack pixels; FP denotes false positives—that is, pixels labeled as noncrack pixels in the ground truth are incorrectly detected as crack pixels; FN represents false negatives—that is, pixels labeled as crack pixels in the ground truth are incorrectly detected as noncrack pixels. Average precision, recall, and F-measure achieved by the proposed method were 92.6, 85.1, and 88.7%, respectively.

Discussion

Research Contributions

The contribution of this study is twofold. First, by using a steerable filter with two rotatable tails, crack segments with high curvature and complicated patterns can be captured, leading to an accurate crack saliency map. Via a region-based active contour model that is implemented using the level set method, the intensity inhomogeneity along a crack is considered in the scale-controllable local region.

Second, the proposed method generates a coarse crack region from the crack saliency map and initializes the active contour model using that coarse crack region, which overcomes the limitation of initial contour selection that prevails in many active contour models. The segmentation performance of active contour models largely depends on the values of parameters. The proposed method roughly estimates the crack properties from the crack saliency map, upon which the parameters of the active contour model are self-adjusted. This treatment improves the efficiency and effectiveness of crack segmentation.

Comparison with the State of the Art

Many studies reported the performance of their methods in crack detection and segmentation. Depending on the data collection method, signal-to-noise ratio, crack complexity, and algorithm, performance varies. In 2D crack detection and segmentation, Ouma and Hahn (2016) reported an average precision of 91.25%, a recall of 80.42%, and a F-measure of 85.49%. Zou et al. (2012) achieved a precision of 79%, a recall of 92%, and a F-measure of 85%. The performances reported in these two studies are among the highest in the literature. Given that the proposed method achieved a precision of 92.6%, a recall of 85.1%, and a F-measure of 88.7%, it can be concluded that it is at least comparable with the state of the art. It is acknowledged that the same set of images should be used to compare all methods, assess their performance, and determine their advantages and disadvantages in varying circumstances. This requires direct access to both data and programs/codes/algorithms. Further efforts are needed to prepare a benchmark data set and manage the access to tools created in all studies.

From a qualitative perspective, the authors believe that the proposed method can complement existing methods in two aspects. First, because of the lack of explicit consideration of complex crack patterns, many existing methods do not show promising performance in segmenting complex cracks such as block and alligator cracks. Moreover, the images being tested sometimes contain only simple cracks such as longitudinal and transverse cracks that are straightforward to detect and segment. In this study, because the majority of crack segments are captured, one can visually observe that the test images contain very complex cracks and that the crack segmentations are satisfactory. In this regard, the proposed method is a promising alternative when there are many complex cracks needing segmentation.

Second, as reported in Ouma and Hahn (2016), their method sometimes is not sufficient to detect cracks with inhomogeneous intensities and poor continuity. In the proposed method, the shifted and rotatable tails in the matched filtering and the scale-controllable local region in the active contour model are specifically leveraged to address the challenges for which existing methods are not suitable.

Limitations and Future Research

There are some limitations in the proposed method which deserve further research. First, this study focused on the processing of 2D images for pavement crack detection and segmentation. Some misleading objects such as oil stains and tire marks may result in false positives because oil stains and tire marks present characteristics similar to those of cracks in 2D images. Techniques have been introduced to obtain 3D pavement data. However, Huang et al. (2014) pointed out that when pavement cracks present no obvious depth changes, 3D profiles may not reflect true information about them, resulting in negative errors. In addition, positive errors are possible because of the inherent limitations of laser scanning technologies. It is acknowledged that both 2D images and 3D data have their respective limitations. Therefore, in the future algorithmic techniques should be created to integrate the processing of 2D images and 3D data for complete and accurate crack detection and segmentation.

Second, some false negatives can be attributed to a number of factors. For instance, the underlying assumptions of steerable matched filtering, such as Gaussian intensity profile, do not hold at some places along a crack curve. In the future, other steerable filters such as a steerable Gabor filter may also be investigated to enhance the proposed method.

Third, the filter size and the offset parameter are fixed as some multiple of the Gaussian variance to calibrate the steerable matched filtering. The relationship of filter size, offset parameter, Gaussian variance, and image resolution can affect crack segmentation. In addition, the values of parameters are experimentally determined in this research, which might not be optimal. Characterizing the optimal configuration of these parameters is challenging, which can be a promising future research direction.

Conclusions

This paper presents a novel method to address three challenges in automatic crack detection and segmentation: (1) low contrast between cracks and surrounding pavement; (2) complicated crack patterns; and (3) intensity inhomogeneity along cracks. A steerable filter with two shifted and rotatable tails is employed to process pavement images, which generates a crack saliency map. Analysis of the crack saliency map leads to a coarse crack region and rough estimates of crack properties. The coarse crack region is then fed into a region-based active contour model for subsequent crack segmentation. The estimated crack properties provide information to

Downloaded from ascelibrary.org by SHENZHEN UNIVERSITY on 01/25/19. Copyright ASCE. For personal use only; all rights reserved.

automatically adjust the parameters of the active contour model, allowing effective and efficient segmentation for various cracks. Sixty-five pavement images with various cracks were tested. The proposed method achieved average precision of 92.6%, recall of 85.1%, and *F*-measure of 88.7%.

Acknowledgments

This research was funded by the National Science Foundation (NSF) via Grant CMMI Nos. 1265895 and 1462638. The authors gratefully acknowledge NSF's support. Any opinions, findings, conclusions, and recommendations expressed in this paper are those of the authors and do not necessarily reflect the views of NSF, Purdue University, and the Georgia Institute of Technology.

References

Alekseychuk, O. (2006). "Detection of crack-like indications in digital radiography by global optimisation of a probabilistic estimation function." Ph.D. thesis, Bundesanstalt fuer Materialforschung und -pruefung, Berlin.

ASCE. (2013). *2013 report card for America's infrastructure*, Washington, DC, 1–74.

Cord, A., and Chambon, S. (2012). "Automatic road defect detection by textural pattern recognition based on AdaBoost." *Comput. Aided Civil Infrastruct. Eng.*, 27(4), 244–259.

FHWA (Federal Highway Administration). (2015). "National performance management measures; assessing pavement condition for the National Highway Performance Program and bridge condition for the National Highway Performance Program." *Federal Register*, 80(2), 326–393.

Freeman, W. T., and Adelson, E. H. (1991). "The design and use of steerable filters." *IEEE Trans. Pattern Anal. Mach. Intell.*, 13(9), 891–906.

Gavilán, M., et al. (2011). "Adaptive road crack detection system by pavement classification." *Sensors*, 11(10), 9628–9657.

Guan, H., et al. (2015). "Iterative tensor voting for pavement crack extraction using mobile laser scanning data." *IEEE Trans. Geosci. Remote Sens.*, 53(3), 1527–1537.

Huang, J., Liu, W., and Sun, X. (2014). "A pavement crack detection method combining 2D with 3D information based on Dempster-Shafer theory." *J. Comput. Aided Civil Infrastruct. Eng.*, 29(4), 299–313.

Huang, Y., and Xu, B. (2006). "Automatic inspection of pavement cracking distress." *J. Electr. Imaging*, 15(1), 013017.

Jacob, M., and Unser, M. (2004). "Design of steerable filters for feature detection using canny-like criteria." *IEEE Trans. Pattern Anal. Mach. Intell.*, 26(8), 1007–1019.

Jiang, C., and Tsai, Y. J. (2015). "Enhanced crack segmentation algorithm using 3D pavement data." *J. Comput. Civil Eng.*, 10.1061/(ASCE)CP.1943-5487.0000488, 04015050.

Kamaliardakani, M., Sun, L., and Ardakani, M. K. (2014). "Sealed-crack detection algorithm using heuristic thresholding approach." *J. Comput. Civil Eng.*, 30(1), 04014110.

Koch, C., Jog, G. M., and Brilakis, I. (2012). "Automated pothole distress assessment using asphalt pavement video data." *J. Comput. Civil Eng.*, 27(4), 370–378.

Li, C., Kao, C. Y., Gore, J. C., and Ding, Z. (2008). "Minimization of region-scalable fitting energy for image segmentation." *IEEE Trans. Image Process.*, 17(10), 1940–1949.

Li, G., He, S., Ju, Y., and Du, K. (2014). "Long-distance precision inspection method for bridge cracks with image processing." *Autom. Constr.*, 41, 83–95.

Li, Q., and Liu, X. (2008). "Novel approach to pavement image segmentation based on neighboring difference histogram method." *Proc., Congress on Image and Signal Processing*, IEEE, New York, 792–796.

Li, Q., Zou, Q., Zhang, D., and Mao, Q. (2011). "FoSA: F* seed-growing approach for crack-line detection from pavement images." *Image Vision Comput.*, 29(12), 861–872.

Lins, R. G., and Givigi, S. N. (2016). "Automatic crack detection and measurement based on image analysis." *IEEE Trans. Instrum. Meas.*, 65(3), 1–8.

McGhee, K. H. (2004). "Automated pavement distress collection techniques." *National Cooperative Highway Research Program Synthesis 334*, Transportation Research Board, Washington, DC.

Mukherjee, S., and Acton, S. T. (2015). "Oriented filters for vessel contrast enhancement with local directional evidence." *Proc., IEEE 12th Int. Symp. on Biomedical Imaging*, IEEE, New York, 503–506.

Nejad, F. M., and Zakeri, H. (2011). "An optimum feature extraction method based on wavelet–radon transform and dynamic neural network for pavement distress classification." *Expert Syst. Appl.*, 38(8), 9442–9460.

Nguyen, H. N., Kam, T. Y., and Cheng, P. Y. (2014). "An automatic approach for accurate edge detection of concrete crack utilizing 2D geometric features of crack." *J. Signal Process. Syst.*, 77(3), 221–240.

Nishikawa, T., Yoshida, J., Sugiyama, T., and Fujino, Y. (2012). "Concrete crack detection by multiple sequential image filtering." *Comput. Aided Civil Infrastruct. Eng.*, 27(1), 29–47.

Oliveira, H., and Correia, P. L. (2013). "Automatic road crack detection and characterization." *IEEE Trans. Intell. Transp. Syst.*, 14(1), 155–168.

Oliveira, H., and Lobato Correia, P. (2009). "Automatic road crack segmentation using entropy and image dynamic thresholding." *Proc., 17th European Signal Processing Conf.*, IEEE, New York, 622–626.

Osher, S., and Sethian, J. A. (1988). "Fronts propagating with curvature-dependent speed: Algorithms based on Hamilton-Jacobi formulations." *J. Comput. Phys.*, 79(1), 12–49.

Otsu, N. (1975). "A threshold selection method from gray-level histograms." *Automatica*, 11(285–296), 23–27.

Ouma, Y. O., and Hahn, M. (2016). "Wavelet-morphology based detection of incipient linear cracks in asphalt pavements from RGB camera imagery and classification using circular radon transform." *Adv. Eng. Inf.*, 30(3), 481–499.

Prasanna, P., et al. (2016). "Automated crack detection on concrete bridges." *IEEE Trans. Autom. Sci. Eng.*, 13(2), 591–599.

Radopoulou, S. C., and Brilakis, I. (2016). "Automated detection of multiple pavement defects." *J. Comput. Civil Eng.*, 10.1061/(ASCE)CP.1943-5487.0000623, 04016057.

Sun, L., Kamaliardakani, M., and Zhang, Y. (2015). "Weighted neighborhood pixels segmentation method for automated detection of cracks on pavement surface images." *J. Comput. Civil Eng.*, 10.1061/(ASCE)CP.1943-5487.0000488, 04015021.

Tsai, Y. C., Jiang, C., and Huang, Y. (2012). "Multiscale crack fundamental element model for real-world pavement crack classification." *J. Comput. Civil Eng.*, 28(4), 04014012.

Tsai, Y. C., Kaul, V., and Mersereau, R. M. (2009). "Critical assessment of pavement distress segmentation methods." *J. Transp. Eng.*, 136(1), 11–19.

Tsai, Y. C. J., and Li, F. (2012). "Critical assessment of detecting asphalt pavement cracks under different lighting and low intensity contrast conditions using emerging 3D laser technology." *J. Transp. Eng.*, 138(5), 649–656.

Yeum, C. M., and Dyke, S. J. (2015). "Vision-based automated crack detection for bridge inspection." *Comput. Aided Civil Infrastruct. Eng.*, 30(10), 759–770.

Ying, L., and Salari, E. (2010). "Beamlet transform-based technique for pavement crack detection and classification." *Comput. Aided Civil Infrastruct. Eng.*, 25(8), 572–580.

Zalama, E., Gómez-García-Bermejo, J., Medina, R., and Llamas, J. (2014). "Road crack detection using visual features extracted by Gabor filters." *Comput. Aided Civil Infrastruct. Eng.*, 29(5), 342–358.

Zhou, J., Huang, P. S., and Chiang, F. P. (2006). "Wavelet-based pavement distress detection and evaluation." *Opt. Eng.*, 45(2), 027007.

Zou, Q., Cao, Y., Li, Q., Mao, Q., and Wang, S. (2012). "CrackTree: Automatic crack detection from pavement images." *Pattern Recognit. Lett.*, 33(3), 227–238.

Downloaded from ascelibrary.org by SHENZHEN UNIVERSITY on 01/25/19. Copyright ASCE. For personal use only; all rights reserved.